

Journal Section: Neurobiology of Disease

**Evolution of Synchrony Dynamics across Brain Structures in Limbic Epilepsy  
Varies Between the Initiation and Termination Phase of Seizures**

*Abbreviated title:* Synchrony dynamics during seizure phases

Tiwalade Sobayo<sup>a,\*</sup>, Ananda S. Fine<sup>b,\*</sup>, Elizabeth Gunnar<sup>a</sup>, Christine Kazlauskas<sup>a</sup>, David Nicholls<sup>c</sup>, and David J. Mogul<sup>a,b</sup>

<sup>a</sup> Illinois Institute of Technology, Department of Biomedical Engineering, 3255 South Dearborn Street, Wishnick Hall, Room 314, Chicago, IL 60616-3793, United States

<sup>b</sup> University of Illinois, Department of Bioengineering, Medical Scientist Training Program, Chicago, IL, United States

<sup>c</sup> University of Illinois, Department of Mathematics, Statistics & Computer Science, Chicago, IL, United States

\* Both authors contributed equally to this research.

Corresponding author: D.J. Mogul  
Illinois Institute of Technology,  
Department of Biomedical Engineering,  
Wishnick Hall, Room 314,  
3255 South Dearborn Street,  
Chicago, IL 60616-3793, United States  
[mogul@iit.edu](mailto:mogul@iit.edu) / 1-312-567-3873 (Tel)

Number of text pages: 27

Number of figures and tables: 9

Number of words for Abstract: 249

Number of words for Introduction: 383

Number of words for Discussion: 945

## **ABSTRACT**

Neuronal populations in the brain achieve levels of synchronous electrophysiological activity as a consequence of both normal brain function as well as during pathological states such as epileptic seizures. Understanding the nature of how synchrony and the dynamics of neuronal oscillators in the brain evolve from normal to the diseased state is a critical component towards decoding such complex behaviors. Controversies have arisen from previous studies that tried to assess the dynamics of the brain during seizures. In this study, we sought to develop a more in-depth understanding of the multi-site dynamics underlying the evolution of seizures in limbic epilepsy by analyzing oscillators in recordings of local field potentials from three subcortical nuclei (bilateral hippocampi and anteromedial thalamus) that are part of the Papez circuit in a kainic acid (KA) rat model of temporal lobe epilepsy extracted using the empirical mode decomposition (EMD) technique. EMD is an adaptive and non-linear decomposition of time series into a set of finite oscillatory components. Oscillator frequencies, power, and phase synchrony were assessed within and between sites as seizures evolved. Most notably, consistent patterns of low-frequency (~35 Hz) synchrony occurred transiently during early-stage ictogenesis between thalamus and both hippocampi; in contrast, higher frequency (~120 Hz) synchrony appeared between thalamus and focal hippocampus as seizures naturally terminated. These multi-site synchrony events may provide a key insight into how synchrony disruption via stimulation could be targeted at specific seizure sites as well as contribute to a better understanding of how brain synchrony evolves in epilepsy.

## **INTRODUCTION**

Epilepsy is a brain disorder characterized by recurrent and spontaneous derangements of normal brain activity, called epileptic seizures (Fisher et al., 2005). More than 50 million people worldwide have epilepsy. Because significant increases in the amplitude of surface electroencephalographic (EEG) recordings are commonly observed in patients undergoing epileptic seizures, research has long been aimed at obtaining a better understanding of the dynamics of brain electrophysiology as seizures evolve. Traditional dogma has asserted that pathologically synchronized activity may underlie seizures; however, recent studies have provided evidence that desynchronization in the brain may instead be an important component during seizures (Netoff and Schiff, 2002; Gutkin et al., 2005; Schindler et al., 2007b).

Considerable controversy still exists concerning the mechanisms by which seizures arise, including the relevance of high frequency oscillations in seizure pathology. Some studies have suggested that ictogenesis in focal epilepsies starts with synchronization in an apparent focus that then spreads to other brain structures (Franaszczuk et al., 1998; Jouny et al., 2010). Others have shown evidence that ictogenesis in focal epilepsies involve specific cortical and subcortical networks beyond the focal site (Bartolomei et al., 2001; Spencer, 2002; Gotman, 2008).

The goal of the present study was to explore the multi-site spatiotemporal dynamics underlying seizure evolution in a kainic acid rat model of temporal lobe epilepsy (TLE) using a novel analytical technique that allows for the nonlinear adaptive decomposition of electrophysiological signals into finite oscillatory components. TLE is a common form of focal epilepsy that is associated with seizure onset in one or more of

the temporal limbic structures (Spencer and Spencer, 1994). The circuit of Papez involving both hippocampus and thalamus is one of the major pathways of the limbic system that it is believed to be involved in TLE (Oikawa et al., 2001) and hence presented an important candidate for studying multi-site network dynamics during seizures.

Local field potentials (LFPs) were recorded from electrodes implanted in three subcortical nuclei: the focal hippocampus (FH), the anteromedial thalamus (T), and the contralateral hippocampus (CH) in rats in which KA was focally injected into FH to induce recurrent seizures. Frequencies, power, and measures of phase synchronization between oscillators extracted from LFPs both within and between subcortical structures were calculated. Significant and distinctly different patterns of phase synchrony were observed during ictogenesis and natural seizure termination.

## **METHODS**

### **1. Animals**

Male Sprague-Dawley rats, 48-57 days old and weighing approximately 225-280 gm were used in this study. Experiments were conducted in accordance with the National Institutes of Health for the care and use of laboratory animals.

### **2. Surgery**

Rats were anesthetized by a mixture of Ketamine (70 mg/kg) and Xylazine (2 mg/kg) delivered intraperitoneally. All procedures were performed in a Kopf stereotactic frame (KOPF Model 900, CA, USA). Stereotactic targets were calculated using a stereotactic rat brain atlas (Paxinos and Watson, 2004). Lambda, Bregma and

Sagittal sutures were used as landmarks to navigate to the desired stereotactic points. The skull was perforated using a high speed stereotactic drill (Micromotor™ Drill, Stoelting Co, IL USA) with 1.2-2 mm diameter drill tips. Seven small burr holes were drilled: four were for the positioning of anchor screws and three for the placement of electrodes.

Bipolar electrodes surrounding a single stainless steel injection cannula in one integrated electrode assembly (C315G-MS 303: PlasticsOne, Roanoke, VA, USA) were stereotactically implanted into the CA3 region of the left hippocampus (-3.5 mm Bregma, 2.8 mm lateral, 3.7 mm deep). Bipolar recording electrodes (without cannula) were implanted into the contralateral hippocampus (-3.5 mm Bregma, -2.8 mm lateral, 3.7 mm deep) and anteromedial thalamus (-1.8 mm Bregma, 0.3 mm lateral, 6.1 mm deep). The electrodes were then fixed to the screws and the skull using acrylic dental cement.

### **3. Method and Analysis of EEG recordings**

Following surgery, intracranial EEG signals were recorded at a sampling rate of 2 kHz. Each experiment involved recording one half hour of baseline activity followed by the injection of 3 – 5 nmol kainic acid into the CA3 region of the left hippocampus (n = 6) to induce epileptogenesis. After injection, the internal cannula insert was withdrawn and a stainless steel insert was threaded through the cannula to provide one side of the recording pair. The reference electrode used was the skull stabilization screw most proximal to the electrode assembly.

The raw signals from each of four recorded channels (namely intracranial recordings from the left and the right hippocampii and the anteromedial nucleus of thalamus as well as a subdural electrode covering the hemisphere contralateral to epileptogenic chemical application to provide surface EEG) were decomposed into a

series of intrinsic mode functions (IMFs) using the method of empirical mode decomposition (EMD). The EMD can be characterized as an adaptive, non-linear decomposition that results in a series of intrinsic mode functions (i.e., IMFs) that together comprise the underlying oscillations (or basis functions) within a dataset (Huang et al., 1998; Sweeney-Reed and Nasuto, 2007). The basis functions are determined from the dynamics of the signal itself which may be non-linear and/or non-stationary (Fine et al., 2010).

After a series of intrinsic oscillators is obtained in this way, the instantaneous phase was calculated using the Hilbert analytic signal method (Gabor, 1946). This method is appropriate in this case because the IMFs represent narrowband signals. Unfiltered, multi-component signals will yield a trajectory in the complex plane that has multiple centers of rotation. For an unambiguous determination of phase, the complex trajectory of the analytic signal must have only a single center of rotation which the EMD technique provides.

Once the IMFs are obtained from each channel within a data segment, the strength of the relationships between the oscillators were determined. To accomplish this, the mean phase coherence (Mormann et al., 2000) was calculated to obtain a square symmetric matrix relating the phase of each IMF oscillator obtained from EMD for each five second window of data. This matrix of phase relationships was then treated to eigenvalue decomposition. This method (Allefeld et al., 2007) allows one to extend a bivariate measure of phase coherence into a multivariate measure thereby permitting measures of synchrony across multiple oscillators. Essentially, this decomposition compares the strength of phase relationships between oscillators and clusters them

according to mean fields. For any eigenvalue-eigenvector pair, a phase correlation value may be assigned as the strength of the connection of a given eigenvalue (unique for a given IMF) and an eigenvector (unique for the entire set of IMFs obtained from all channels). Furthermore, each eigenvalue is ordered, with the largest eigenvalue representing the most strongly correlated cluster with the participation of each oscillator in a given cluster quantified by the value of the eigenvector. Those eigenvalues above one are considered significant and the components of their eigenvectors identify participation in the corresponding cluster. In the analysis of our data, only the most significant clusters were analyzed to determine how synchrony dynamics evolve during seizures

#### 4. Analysis of phase synchrony

Given an ensemble of coupled oscillators, in order to analyze the group's collective dynamics and, in particular, to describe synchronization processes, it is convenient to introduce the complex cluster variable  $Z$ :

$$Z = r e^{i\varphi} = \frac{1}{N} \sum_{j=1}^N e^{i\phi_j} \quad (1)$$

where  $\Phi_j$  is the phase of the  $j^{\text{th}}$  oscillator and  $N$  is the number of oscillators (Winfree, 1977; Kuramoto, 1984; Tass, 1999). The quantities  $r$  and  $\varphi$  denote the cluster amplitude and cluster phase at time  $t$ , respectively. The variable  $r$  is also known as mean phase coherence (Mormann et al., 2000) and phase amplitude coherence (Schiff et al., 2005).

The cluster amplitude varies between 0 and 1. As the ensemble becomes more synchronized, the cluster amplitude increases towards unity. The difference in instantaneous cluster amplitude,  $\Delta r$ , was calculated for the length of the entire recording. The variance of  $\Delta r$  (also known as the *phase amplitude dispersion*) was then calculated

using a 100 ms moving window. All the IMFs extracted from the same recording channel were analyzed using this measure in order to access the level of synchrony within a recording channel. As the oscillators become more coherent in phase, the phase amplitude dispersion should decrease.

In order to quantify the level of synchrony across recording channels, we employed the phase locking value (PLV) approach (Lachaux et al., 1999; Sakkalis et al., 2007). For two signals  $x(t)$  and  $y(t)$  of equal time length with instantaneous phases  $\Phi_x(t)$  and  $\Phi_y(t)$  respectively, the PLV bivariate metric is given by:

$$PLV = \left| \frac{1}{N} \sum_{j=1}^N e(i(\phi_x(j\Delta t) - \phi_y(j\Delta t))) \right| \quad (2)$$

where  $\Delta t$  is the sampling period and  $N$  is the number of points in the sampling period of each signal. PLV can vary between 0 and 1 where 1 indicates perfect phase synchronization and 0 indicates no phase synchronization.

For any two different recording channels, the PLVs of multiple pairs of IMFs that reside in the topmost significant cluster were used to construct a PLV matrix. The Euclidean norm (L2 norm) of the columns of the PLV matrix was then taken as a representative of phase synchrony between the channels. This operation reduced the PLV matrix from a  $m \times n$  matrix to a  $1 \times n$  matrix. In order to assess the significance of synchrony as quantified by PLV, we employed the use of phase randomized surrogate data sets. Initially, surrogates were produced using both the phase randomization technique and the more robust Fourier shuffling technique. Our tests on preliminary data showed that both surrogates were giving virtually the same results. We settled on using phase-randomized surrogates because it was computationally faster to generate these.

Twenty surrogate data sets were created for each original data series. Pairs of IMFs possessing PLVs that exceeded the threshold for 95% significance compared to that for surrogates were considered to have statistically significant synchrony.

## **RESULTS**

### **Intracranial seizure activity elicited by hippocampal microinjection of KA:**

Local field potentials (LFPs) were recorded in the anesthetized rat from three locations implicated in limbic seizures as described in the Method's section. Recordings showing 100 sec of electrographic activity at each of the three intracranial electrode sites prior to (baseline) kainic acid (KA) injection and a KA-induced spontaneous seizure are displayed in Figure 1, panels A1 and A2, respectively. High amplitude LFPs were observed spontaneously occurring within 20 minutes after microinjection of KA (20 $\mu$ L) into the CA3 region of the focal hippocampus. In order to clearly identify the ictal period, the Teager Energy (TE) of each LFP time series was calculated for either baseline (panel B1) or KA-induced spontaneous seizure (panel B2). The Teager Energy amplitude was found to be a reliable indicator of the ictal region which provided temporal markers for seizure onset and termination because high amplitude TE was only present when there was high amplitude LFP recordings correlated with KA-induced seizure activity.

Since seizures are generally thought to represent aberrantly synchronized neural activity, we sought to develop a set of algorithms to accurately access and quantify this synchrony. Empirical Mode Decomposition (EMD) was used to decompose the raw time series signals into a finite collection of oscillators known as intrinsic mode functions (IMFs). Figure 2 shows the collection of IMFs obtained from the decomposition of a LFP

from the focal hippocampus recorded during the appearance of a spontaneous KA-induced seizure. Note that linear summation of the IMFs produces the original time series signal. EMD was chosen over other techniques such as Fourier because it decomposes a time series into a finite number of orthogonal oscillators without assuming either linearity or stationarity of the underlying system responsible for the signal.

**Dominant oscillator frequencies during baseline activity and spontaneous seizures:**

The Hilbert analytic signal was constructed for each IMF in order to calculate the instantaneous phase for each. Moving averages of IMF frequencies were calculated by taking the absolute mean of the time derivative of the instantaneous phase of each IMF over 1 sec intervals. In order to better visualize activity across a broad frequency range, the IMF frequencies are displayed in two separate plots: (i) high frequency oscillators (defined as IMF's with a frequency  $\geq 30$  Hz) and (ii) low frequency oscillators (IMF's with a maximum frequency  $< 30$  Hz). The frequency of 30 Hz was used as the differentiation between high and low frequency oscillators in part because many researchers (e.g., Kohling et al., 2000; Fisahn, 2005; Lehmkuhle et al., 2009) have reported that oscillators in the gamma band and above play an important role in epilepsy. Figure 3A shows the frequencies extracted from the focal hippocampus, thalamus, and contralateral hippocampus during a baseline recording from one of the experimental animals prior to KA injection. Figure 3B shows the extracted IMF frequencies of the same animal in which KA-induced spontaneous seizure activity occurs. During the baseline, the frequency of oscillator activity remains relatively unchanged. However, at the onset of the ictal period (as indicated by significant increase in Teager energy), there is a coincident drop in the frequencies of IMFs with pre-ictal frequencies greater than 600

Hz while there is a rise in the frequencies of IMFs with pre-ictal frequencies less than 600 Hz. At the end of the ictal period, the frequencies of the IMFs return to their pre-ictal values. This convergence of IMF frequencies is shown more clearly by the large drop in the variance of the frequencies during the ictal period that was never present during baseline recordings (Fig 4).

**The power of IMF oscillators increases significantly during seizures:**

In order to better assess the nature of the synchrony occurring during a seizure, the power of the IMFs extracted from each recording site was calculated in order to determine if the high energy activity seen during the ictal period could be attributed to an increase in the power of individual IMFs as opposed to simply an increase in IMF synchrony. The instantaneous power of an IMF was calculated by taking the square of its amplitude. The average power was then calculated by taking the mean of the instantaneous power over a 1 sec interval. In Figure 5A the logarithm of the average power for the first 10 IMFs of a post KA injection recording obtained from the focal hippocampus of an animal experiencing two spontaneous seizures is plotted as a function of time. Plots were separated into high frequency (panel A2) and low frequency (panel A3) IMFs as defined previously. Each colored line is representative of one IMF. The power of the IMFs increase during the seizure in comparison to the pre- and post-ictal periods. A comparison of the logarithm of the average power for the first 10 IMFs across all post KA injection recordings (n = 21 seizures) reveal a significant increase in power during the ictal period (one-way ANOVA;  $p < 10^{-5}$ ). Figure 5, panel B shows the grand averages of the logarithm of the average power for these IMFs from the focal hippocampus, thalamus, and contralateral hippocampus for all post KA injection seizure

recordings. The mean power during the ictal period ranges from approximately 5 to 8 times the mean power during the pre-ictal or post-ictal periods indicating that at least some component of overall increase in seizure energy is due to increases in oscillator amplitudes at each of the three different structures.

**Phase synchrony assessed *within* recording sites:**

The Hilbert analytic signal was constructed for each IMF in order to calculate the instantaneous phase for each oscillator. The instantaneous phases for all IMFs that belong to the same recording site were then used to calculate *phase amplitude dispersions* ( $\text{var}[\Delta r]$ ) as a way of quantifying phase synchrony within each recording site in the brain. In order to compare how synchrony evolved, five temporal categories for each seizure event in all post KA injection recordings were created based on evolution of the Teager energy: namely, pre-ictal, initiation, mid-seizure, termination, and post-ictal. Figures 6A, 6B and 6C show the phase amplitude dispersion for the focal hippocampus, thalamus, and contralateral hippocampus respectively. Phase amplitude dispersion significantly decreased in all three recording sites (ANOVA;  $p < 10^{-4}$  for all three sites) as the middle of the seizure period was approached followed by an increase as seizures evolved towards termination. This pattern of dynamics is consistent with an overall increase in the synchrony of electrophysiological activity within each structure during limbic seizures and is thus consistent with seizures as hypersynchronous events.

**Phase synchrony assessed *between* recording sites:**

The ability to identify discrete oscillators in the electrophysiological behavior recorded in each brain structure permitted an assessment of how interregional synchrony evolved during the different phases of activity in an epileptic rat. In order to better

understand the spatiotemporal dynamics occurring during a seizure, synchrony *across* recording sites was evaluated. To accomplish this, the phase locking value (PLV) between pairs of sites was calculated. IMFs from all the recording sites were clustered to find groups of two or more oscillators whose dynamic behavior may be correlated. Significantly synchronized clusters were identified through eigenvalue decomposition as described in the Method's section. The top (or most) significantly synchronized clusters were identified and PLVs were calculated for pairs of IMFs based on three groupings: (i) IMFs from focal hippocampus *vs.* thalamus, (ii) IMFs from thalamus *vs.* contralateral hippocampus, and (iii) IMFs from focal hippocampus *vs.* contralateral hippocampus. In order to assess the statistical significance of phase locking events, surrogates (as described in Methods) were employed.

Figure 7 is a plot of the patterns of phase locking across pairs of structures for a post KA injection recording containing a seizure. The PLVs for the different combination of pairs of recording site for all seizures were analyzed to identify continuous time periods where the phase locking exceeded 95% significance. Time periods with a minimum length of time of 100 ms were selected and the frequencies of both oscillators were identified. A threshold of 100 ms was used for the length of phase locking because it is longer than the typical time course that has been observed for excitatory post-synaptic currents in rat hippocampal neurons (Mennerick and Zorumski, 1995; Ivenshitz and Segal, 2006). In all of the seizures, there was significant phase locking (defined as a PLV that exceeded the 95% significance threshold derived from surrogates for at least 100msec) between the focal hippocampus and the thalamus in the run up to the ictal activity. There are fewer occurrences of significant phase locking

during the seizure; and then there is re-emergence of significant phase locking at the termination of the ictal activity. The pattern of significant phase locking between the focal hippocampus and the contralateral hippocampus and between the thalamus and contralateral hippocampus varies considerably from seizure to seizure.

The result of this analysis for typical seizure events from the same animal is shown in Figure 8. A synchrony analysis of activity during a segment of the baseline period before KA injection is shown in figure 8A. Teager energy is shown for each of the three recording periods in order to differentiate baseline from pre-ictal or ictal activity. As in figure 3, analytical results have been divided into low frequency ( $f \leq 30\text{Hz}$ ) and high-frequency ( $f > 30\text{Hz}$ ) plots. Note that only very low frequency synchrony ( $f < 10\text{Hz}$ ) was evident in a non-seizing anesthetized animal prior to KA exposure. Panels B and C in figure 8 represent different spontaneous seizure events in the same animal. Low frequency synchrony was observed throughout each recording period shown (figure 8; panels B2 & C2) irrespective of seizure activity. Some higher frequency synchrony ( $f \approx 25\text{Hz}$ ) was sometimes seen but not reliably for all seizures in a given animal or between animals. However, more significant synchrony correlated closely to seizure activity was seen in the high frequency range. For a majority of the seizures (19 out of 21), a 1:1 frequency locking in the 30-50 Hz frequency range was observed between all three sites just prior to the beginning of the full-blown seizure as determined by the Teager energy (panels B3 and C3). Because this synchrony appears prior to the high-amplitude seizure onset, one might conclude that this dynamic is important to the generation of a seizure and not simply a consequence of it. In contrast, a 1:1 frequency locking in the 120-160 Hz frequency range was observed primarily

between the focal hippocampus and the thalamus as the seizure naturally terminates. This dynamic was reliably observed across seizures within the same animal and between animals although differences in frequency of locking prior to termination were seen possibly because the epilepsies generated via KA injection may not have been precisely identical in underlying mechanisms. To our knowledge, this is the first evidence of clear interregional synchrony between these structures at well-defined frequencies and seizure states in an *in vivo* animal model of limbic epilepsy.

## **DISCUSSION**

The aim of this study was to investigate the pattern of spatiotemporal dynamics which underlie spontaneous ictal activity during seizure evolution in the kainic acid rat model of temporal lobe epilepsy. Understanding how these dynamics evolve can provide not only a greater overall description of the electrophysiological mechanisms underlying seizures but may also yield important insights crucial to clinical management of the disease. Current diagnostic protocols as part of pre-surgical work-up for patients undergoing ablation therapy for disruption of ictogenesis could be greatly assisted by better understanding how structures in the brain interact with a putative seizure focus to induce seizure initiation. Such understanding of the dynamics might also provide important new insights for more accurate seizure prediction. Furthermore, better understanding of how brain circuitry interacts during the natural termination of a seizure may also provide key insights as to how exogenous manipulation of brain states such as through electrical stimulation might achieve greater efficacy. The method of empirical mode decomposition (EMD) was employed in our analysis because it is an adaptive

decomposition which does not require assumptions of linearity or stationarity of the dataset unlike Fourier analysis. Another advantage to using EMD is that it decomposes the original signal into a finite set of oscillatory components known as the intrinsic mode functions (IMFs) with well-defined centers of rotation which provides us with specific dynamic targets of activity to both analyze for changes as a consequence of the disease as well as for potential disruption.

The frequencies of the IMF oscillators tended toward convergence during ictal events. A decrease in the frequency of very high frequency ( $f > 600\text{Hz}$ ) IMFs along with increases in the frequency of low frequency IMFs were observed. Similar increases in the frequency of low frequency oscillators ( $f < 60\text{Hz}$ ) during a seizure have been reported using different analysis techniques (Hsu et al., 2010). Furthermore, an increase in the power of all IMFs during the ictal period was observed when compared to the pre-ictal and post-ictal period suggesting that to the extent that these oscillators represent regional neuronal activity, seizures brought about increased neuronal activity and not just increased synchrony.

Synchrony between oscillators from within the same subcortical nucleus as well as synchrony between oscillators from pairs of different subcortical nuclei in the seizure network were calculated. Seemingly conflicting results were obtained when we examined the synchrony between the oscillators. It was found that the synchrony between oscillators extracted from the same recording sites increased during a seizure while oscillators from separate recording sites displayed significant and persistent synchronization at seizure initiation and termination. This suggests that epileptic seizures are characterized by increasing synchrony within each subcortical nucleus; however,

there is reduced synchrony across the seizure circuit. This result is very similar to what has been shown about the difference in local and distant phase synchronization in generalized seizures in humans (Garcia Dominguez et al., 2005). This also supports the idea that synchronization in the brain differs based on the spatial scale one is considering.

In Figure 9, characteristic patterns that emerged during 10 second windows at the start of the ictal activity and as seizures naturally terminated are diagrammed. The network synchronization that is coincident with seizure termination is interesting in that it may offer insight into how to design and implement seizure perturbation protocols such as electrical deep brain stimulation aimed at seizure disruption. Three different patterns were observed as the seizures began to terminate: (i) over half of the seizures display locking between the focal hippocampus and the thalamus (60%); (ii) 7% display locking initially between the thalamus and the contralateral hippocampus; and (iii) 25% display locking between the focal hippocampus and the contralateral hippocampus. By the end of the 10 sec window, all of the seizures show direct or indirect phase locking between the focal hippocampus and the thalamus.

Both the thalamus and the hippocampus have been used as targets for brain stimulation as treatment for intractable, medication-resistant focal epilepsy (Jobst et al., 2010). However, trials have only looked at single site stimulation at one of both structures and they have yielded inconsistent results. Furthermore, increasing synchronization in the brain has recently been proposed to be one possible way of terminating seizures (Schindler et al., 2007a). These observations along with the findings of our study suggest that an electrical stimulation paradigm involving simultaneous stimulation of both the focal hippocampus and the thalamus might be more effective in

limbic seizure disruption than one that involves stimulation at only the hippocampus or the thalamus.

It is unknown whether the IMFs from EMD represent actual physiological oscillators or merely depict the phase dynamics of one or more network oscillations. This may cause uncertainties with direct physical interpretation of the IMFs obtained from the decomposition although it is unlikely to interfere with synchrony analysis. However, more to the point is that the standard frequency analysis of brain electrographic activity using Fourier analysis has commonly produced analytical summaries of brain activity in frequency bands (i.e., theta, beta bands, etc.) whose physiological relevance is also not well understood but whose dynamics characterization has proved invaluable to understanding correlative relevance of brain behavior. Furthermore, most other decomposition methods, to our knowledge, depend on assumptions of some *a priori* determined oscillator waveforms underlying the time series signals that relies on assumptions of linearity or stationarity of neuronal network electrophysiology that may very well be erroneous. Thus the analytical outcomes using the techniques described in this paper provided discrete oscillator phase and frequency information that offers new insights into inter-site network behavior in the brain during seizures and provides specific spatiotemporal dynamics that may be directly manipulatable by exogenous electrical perturbation.

## **REFERENCES:**

- Allefeld C, Muller M, Kurths J (2007) Eigenvalue decomposition as a generalized synchronization cluster analysis. *International Journal of Bifurcation and Chaos* 17:3493-3497.
- Bartolomei F, Wendling F, Bellanger JJ, Regis J, Chauvel P (2001) Neural networks involving the medial temporal structures in temporal lobe epilepsy. *Clin Neurophysiol* 112:1746-1760.
- Fine AS, Nicholls DP, Mogul DJ (2010) Assessing instantaneous synchrony of nonlinear nonstationary oscillators in the brain. *J Neurosci Methods* 186:42-51.
- Fisahn A (2005) Kainate receptors and rhythmic activity in neuronal networks: hippocampal gamma oscillations as a tool. *J Physiol* 562:65-72.
- Fisher RS, van Emde Boas W, Blume W, Elger C, Genton P, Lee P, Engel J, Jr. (2005) Epileptic seizures and epilepsy: definitions proposed by the International League Against Epilepsy (ILAE) and the International Bureau for Epilepsy (IBE). *Epilepsia* 46:470-472.
- Franaszczuk PJ, Bergey GK, Durka PJ, Eisenberg HM (1998) Time-frequency analysis using the matching pursuit algorithm applied to seizures originating from the mesial temporal lobe. *Electroencephalogr Clin Neurophysiol* 106:513-521.
- Gabor D (1946) Theory of Communication. *J IEEE London* 93:429-457.
- Garcia Dominguez L, Wennberg RA, Gaetz W, Cheyne D, Snead OC, 3rd, Perez Velazquez JL (2005) Enhanced synchrony in epileptiform activity? Local versus distant phase synchronization in generalized seizures. *J Neurosci* 25:8077-8084.

- Gotman J (2008) Epileptic networks studied with EEG-fMRI. *Epilepsia* 49 Suppl 3:42-51.
- Gutkin BS, Ermentrout GB, Reyes AD (2005) Phase-response curves give the responses of neurons to transient inputs. *J Neurophysiol* 94:1623-1635.
- Hsu D, Hsu M, Grabenstatter HL, Worrell GA, Sutula TP (2010) Time-frequency analysis using damped-oscillator pseudo-wavelets: Application to electrophysiological recordings. *J Neurosci Methods* 194:179-192.
- Huang NE, Shen Z, Long SR, Wu MC, Shih HH, Zheng Q, Yen N-C, Liu HH (1998) The empirical mode decomposition and the Hilbert spectrum for nonlinear and non-stationary time series analysis. *Proceedings of the Royal Society London* 454:903-995.
- Ivenshitz M, Segal M (2006) Simultaneous NMDA-dependent long-term potentiation of EPSCs and long-term depression of IPSCs in cultured rat hippocampal neurons. *J Neurosci* 26:1199-1210.
- Jobst BC, Darcey TM, Thadani VM, Roberts DW (2010) Brain stimulation for the treatment of epilepsy. *Epilepsia* 51 Suppl 3:88-92.
- Jouy CC, Bergey GK, Franaszczuk PJ (2010) Partial seizures are associated with early increases in signal complexity. *Clin Neurophysiol* 121:7-13.
- Kohling R, Vreugdenhil M, Bracci E, Jefferys JG (2000) Ictal epileptiform activity is facilitated by hippocampal GABAA receptor-mediated oscillations. *J Neurosci* 20:6820-6829.
- Kuramoto Y (1984) *Chemical oscillations, waves and turbulence*. Berlin: Springer-Verlag.

- Lachaux JP, Rodriguez E, Martinerie J, Varela FJ (1999) Measuring phase synchrony in brain signals. *Hum Brain Mapp* 8:194-208.
- Lehmkuhle MJ, Thomson KE, Scheerlinck P, Pouliot W, Greger B, Dudek FE (2009) A simple quantitative method for analyzing electrographic status epilepticus in rats. *J Neurophysiol* 101:1660-1670.
- Mennerick S, Zorumski CF (1995) Presynaptic influence on the time course of fast excitatory synaptic currents in cultured hippocampal cells. *J Neurosci* 15:3178-3192.
- Mormann F, Lehnertz K, David P, Elger CE (2000) Mean phase coherence as a measure for phase synchronization and its application to the EEG of epilepsy patients. *Physica D* 144:358 - 369.
- Netoff TI, Schiff SJ (2002) Decreased neuronal synchronization during experimental seizures. *J Neurosci* 22:7297-7307.
- Oikawa H, Sasaki M, Tamakawa Y, Kamei A (2001) The circuit of Papez in mesial temporal sclerosis: MRI. *Neuroradiology* 43:205-210.
- Paxinos G, Watson C (2004) *The rat brain in stereotaxic coordinates*, 5 Edition: Academic Press.
- Sakkalis V, Tsiaras V, Zervakis M, Tollis I (2007) Optimal brain network synchrony visualization: application in an alcoholism paradigm. *Conf Proc IEEE Eng Med Biol Soc* 2007:4285-4288.
- Schiff SJ, Sauer T, Kumar R, Weinstein SL (2005) Neuronal spatiotemporal pattern discrimination: the dynamical evolution of seizures. *Neuroimage* 28:1043-1055.

- Schindler K, Elger CE, Lehnertz K (2007a) Increasing synchronization may promote seizure termination: evidence from status epilepticus. *Clin Neurophysiol* 118:1955-1968.
- Schindler K, Leung H, Elger CE, Lehnertz K (2007b) Assessing seizure dynamics by analysing the correlation structure of multichannel intracranial EEG. *Brain* 130:65-77.
- Spencer SS (2002) Neural networks in human epilepsy: evidence of and implications for treatment. *Epilepsia* 43:219-227.
- Spencer SS, Spencer DD (1994) Entorhinal-hippocampal interactions in medial temporal lobe epilepsy. *Epilepsia* 35:721-727.
- Sweeney-Reed CM, Nasuto SJ (2007) A novel approach to the detection of synchronisation in EEG based on empirical mode decomposition. *J Comput Neurosci* 23:79-111.
- Tass PA (1999) *Phase resetting in medicine and biology : stochastic modelling and data analysis*. Berlin ; New York: Springer Verlag.
- Winfree AT (1977) Phase control of neural pacemakers. *Science* 197:761-763.

## **FIGURE LEGENDS:**

### **Figure 1.**

Intracranial electrographic activity before and after kainic acid (KA) injection. **(A1)**

Baseline recordings of electrographic activity recorded from intracranial electrodes placed in the focal hippocampus, anteromedial thalamus, and contralateral hippocampus.

The *focal* hippocampus is the left hippocampus in which the electrode assembly contains a microcannula for KA injection. **(A2)** Recordings of electrographic activity from the same three sites as in panel A1 but showing evidence of a spontaneous seizure induced by a prior injection of KA. Teager Energy of baseline recordings **(B1)** and of ictal recording **(B2)** gives a clear indication of the approximate time course of a seizure.

### **Figure 2.**

Empirical mode decomposition (EMD) provides a nonlinear nonstationary deconvolution of the electrographic activity recorded in the focal hippocampus into a finite number of oscillators. Intracranial EEG segment containing one spontaneous seizure is shown on top. A 40 sec segment containing the seizure underwent EMD transformation and the first 10 Intrinsic Mode Functions (IMFs) were extracted. The EMD technique (see Methods) extracts the IMF oscillator with the highest frequency first and then progressively lower frequency oscillators. Linear addition of IMFs precisely reproduces the original signal.

**Figure 3.**

Frequencies of IMF oscillators converge during a seizure. Frequency analysis was performed on the IMFs extracted from the electrographic signals recorded in the focal and contralateral hippocampi and anteromedial thalamus under: **(A)** Baseline conditions prior to KA exposure, and **(B)** during a spontaneous seizure following KA injection into the focal hippocampus. For each time period of analysis, the Teager energy (TE) is shown. Display of the analysis has been divided into the top five, high frequency IMFs ( $f > 30\text{Hz}$ ) and low frequency IMFs ( $f \leq 30\text{Hz}$ ). Each IMF is color-coded to permit better visualization of oscillator dynamics over time. The distribution of frequencies was very stable under baseline conditions but during an ictal period, IMFs in both the high and low frequency categories tended toward convergence.

**Figure 4.**

The variance of IMF frequencies significantly reduces during a seizure. The total variance of frequencies of the first ten IMFs extracted from the intracranial signal recorded in focal hippocampus (red), contralateral hippocampus (black) and anteromedial thalamus (green) is shown. Reductions in total variance were larger and more similar between hippocampi than for the thalamus.

**Figure 5.**

Increase in IMF power observed during seizures. **(A)** IMF power was measured in an animal from electrophysiological behavior recorded in the focal hippocampus (FH), anteromedial thalamus (T) and contralateral hippocampus (CH) during two sequential

spontaneous seizures. Panel A1: The Teager Energy of an ictal recording shows the time course of two spontaneous seizures in a KA-rat model. Panel A2 & A3: the time course of the IMF power in the high and low frequency ranges, respectively, as defined earlier. The percentage increase in IMF power is higher in those oscillators with  $f > 30\text{Hz}$ . **(B)** The average power of the first 10 IMFs from each of the three structures being recorded in 11 seizures. The results of all data were averaged within groups as pre-ictal, ictal, and post-ictal periods based on levels of Teager Energy. ANOVA analysis indicated significant increase in power during the ictal period.

**Figure 6.**

Synchrony of oscillators measured within each structure increases as rats evolve into seizures. Average phase amplitude dispersion of all IMFs in **(A)** focal hippocampus, **(B)** anteromedial thalamus, and **(C)** contralateral hippocampus for 21 seizures. The results of all data were averaged within groups as pre-ictal, initiation, mid-seizure, termination, and post-ictal periods. The phase amplitude dispersion achieved its lowest value during the middle of the seizure in all three brain structures.

**Figure 7.**

Phase locking between pairs of structures indicates periods of phase synchrony during a seizure episode. Upper panel: Teager Energy indicates an ictal event containing one spontaneous seizure lasting approximately 70 sec. Paired comparisons of phase locking are shown between focal hippocampus and thalamus (top), focal and contralateral hippocampus (middle), and thalamus and contralateral hippocampus (bottom). For all

PLV plots, a dashed line denotes the 95% significance level of the phase locking value determined using randomized surrogates (see Methods).

**Figure 8.**

The synchrony dynamics of oscillators in different structures in the rat brain exhibit phase locking (PL) as spontaneous seizures evolve. Synchrony dynamics are shown during three ictal periods in the same animal: (A) Baseline conditions prior to exposure to KA, (B) During a single spontaneous seizure, and (C) During a period in which two spontaneous seizures consecutively appeared. The Teager Energy of the focal hippocampus electrical activity is provided at the top of each panel to delineate full-blown seizures from non-ictal activity. Plots show periods of significant phase locking (i.e., >95%) that occur between pairs of brain structures for at least a contiguous 100msec. Because phase locking does not always occur 1:1, the frequency of IMF from each pair is shown (e.g., FT-F indicates significant phase locking between focal hippocampus (F) and thalamus (T) with the focal hippocampus IMF frequency indicated by the symbol noted in the inset key in each frequency plot. Low frequency phase-locking among IMFs during a 10min segment of baseline recording is shown in panel A. High frequency ( $f > 30\text{Hz}$ ) PL is not shown here because none appeared in any of the experiments under pre-KA exposure baseline conditions. In this experiment, PL was only seen at frequencies below 10Hz which was typical. Similar plots of low frequency locking events as in panel A is shown in B2 and C2. As shown, PL prior to or coincident with seizure initiation occurred at  $10\text{Hz} < f < 25\text{Hz}$  although this was not reliably observed within the same seizing animal or between animals. In contrast, significant PL was

reliably seen at higher frequencies coincident with seizure onset or termination (panels B3 & C3). PL events are highlighted by the dashed ovals. During ictogenesis, PL at ~50Hz was frequently observed that did not persist once full-blown seizure onset occurred. Furthermore, natural seizure termination was reliably coincident with seizure locking at frequencies between approximately 130-160Hz.

**Figure 9.**

Schematic of synchronization patterns between brain structure pairs that occurred coincident with seizure initiation or termination. The frequency of the line connecting any two subcortical nuclei represents the frequency range of the oscillators as defined here. Low: 30-100Hz; medium: 100-160Hz; high: >160Hz. The number in the boxes is the percentage of seizures depicting that particular pattern. **(A)** Depictions of the different patterns of significant and persistent phase locking between the three subcortical nuclei coincident with the start of ictal activity. In 80% of the seizures, phase locking occurred between the thalamus and one of the hippocampi in the low frequency range as defined above. Four different permutations of phase locking occurred prior to the full-blown seizure after which no higher frequency synchrony was observed. **(B)** Depictions of the different patterns of significant and persistent phase locking between the three subcortical nuclei in a 10 second window at the natural termination of ictal activity. At seizure termination, medium frequency synchrony was initially observed. This dynamic evolved to include higher frequency PL that sometimes included more regions than initially although it should be noted that, in 82% of the seizure termination incidents, synchrony occurred primarily between thalamus and focal hippocampus.

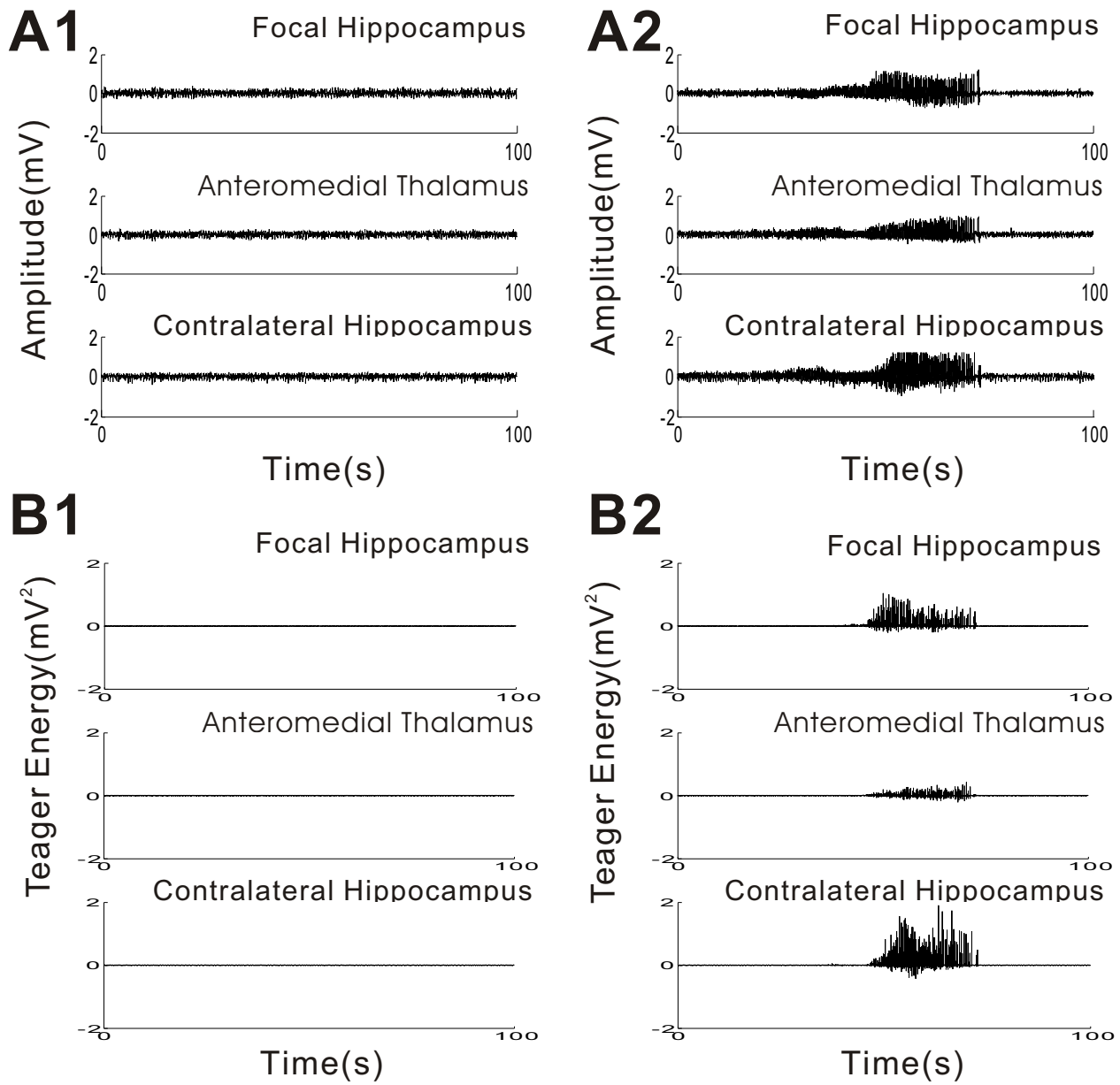


Figure 1

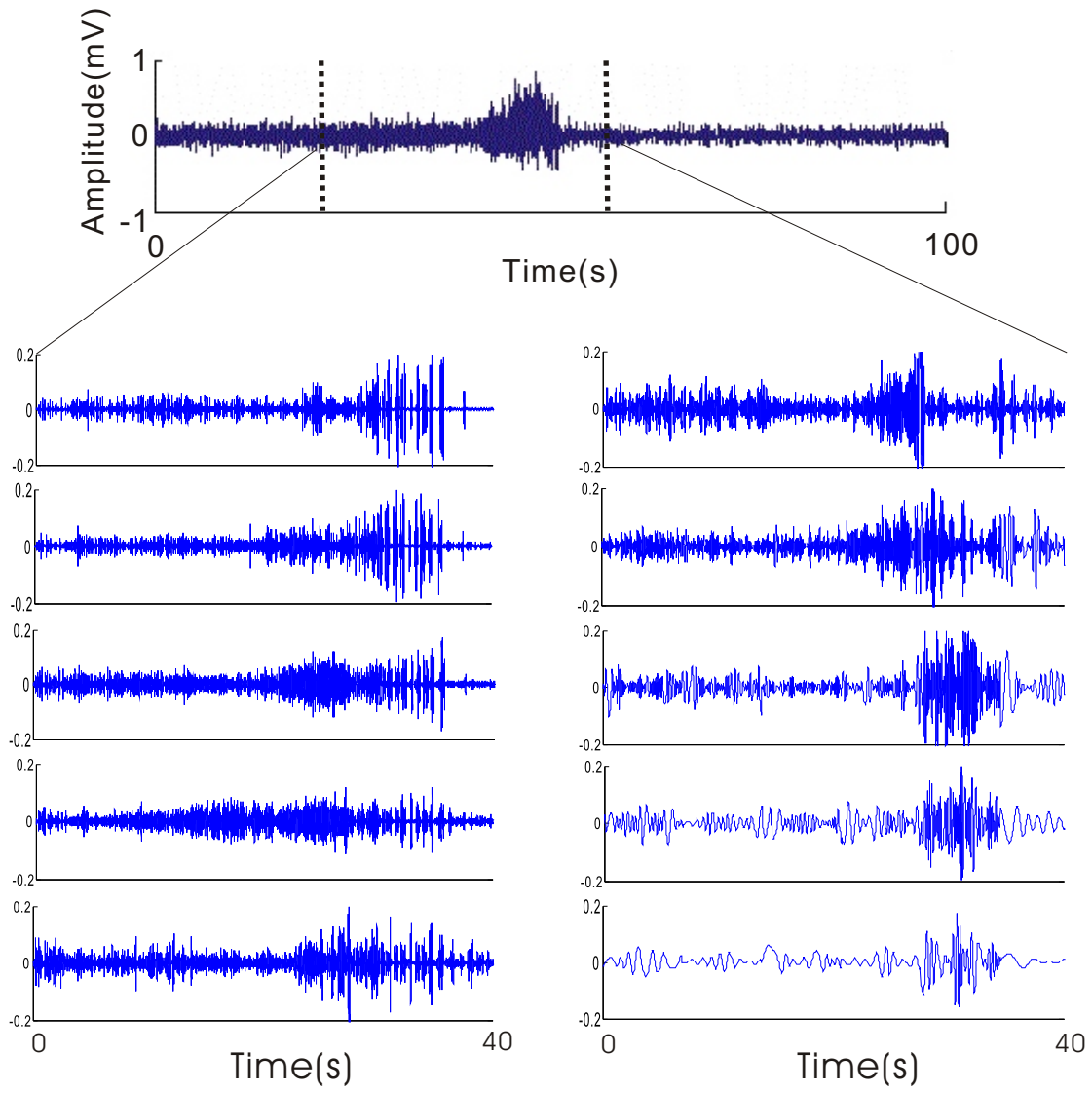


Figure 2

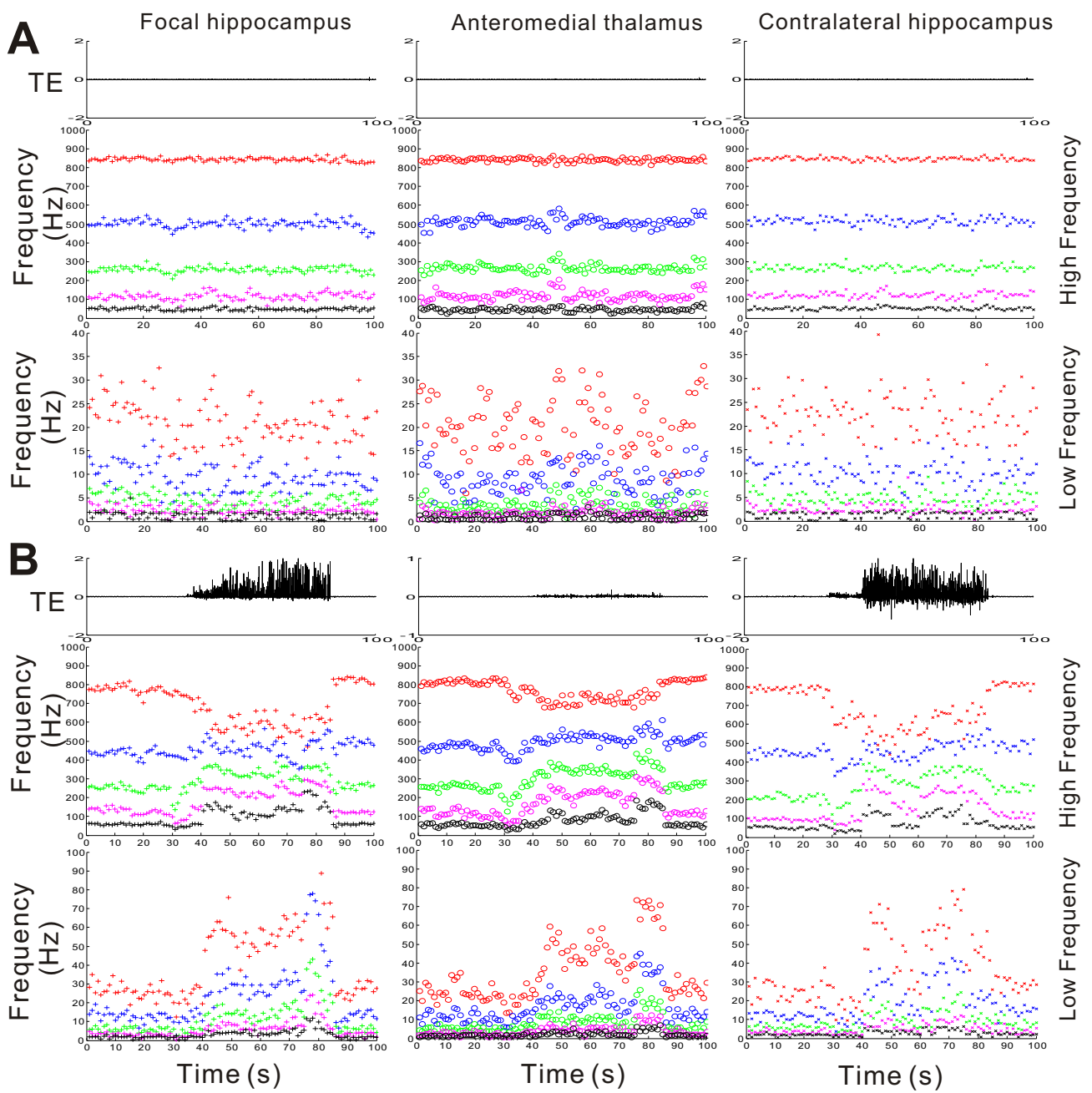


Figure 3

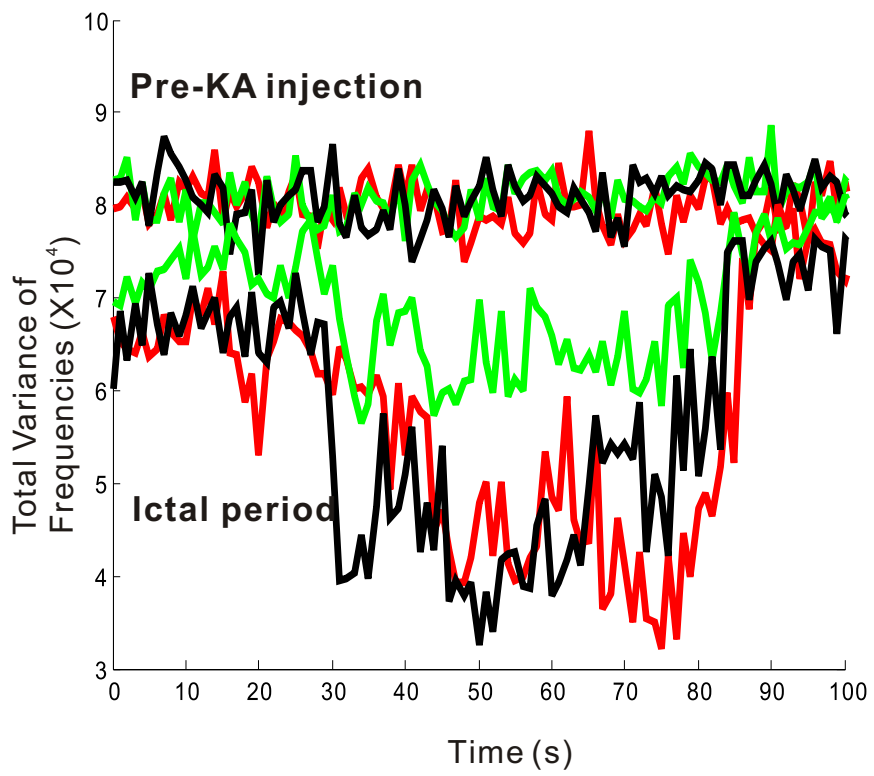
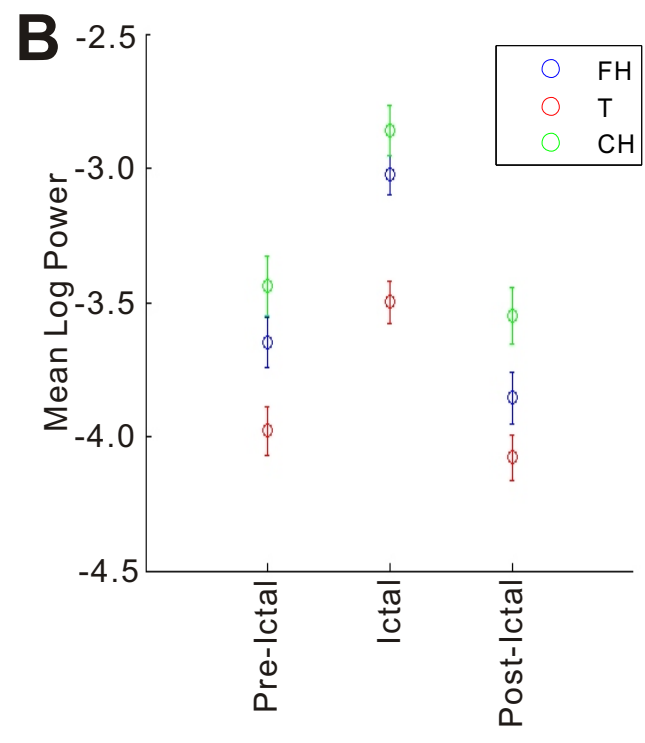
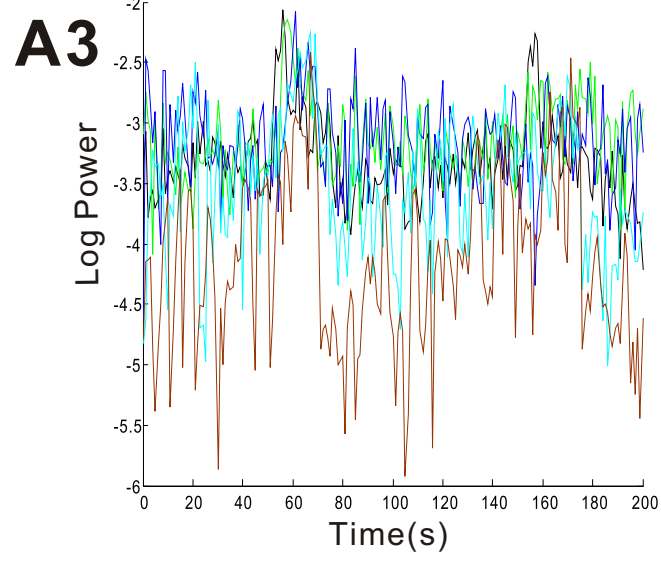
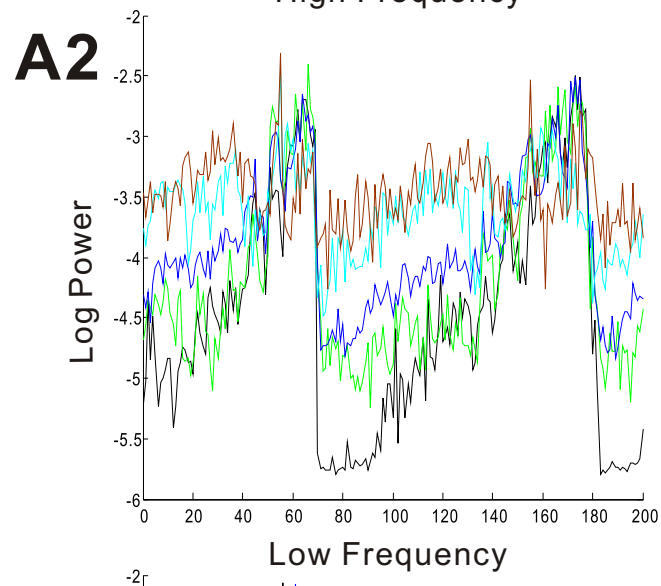
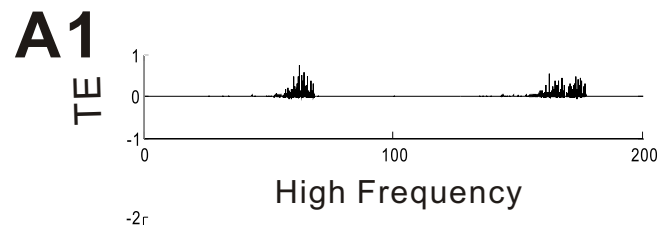


Figure 4



**Figure 5**

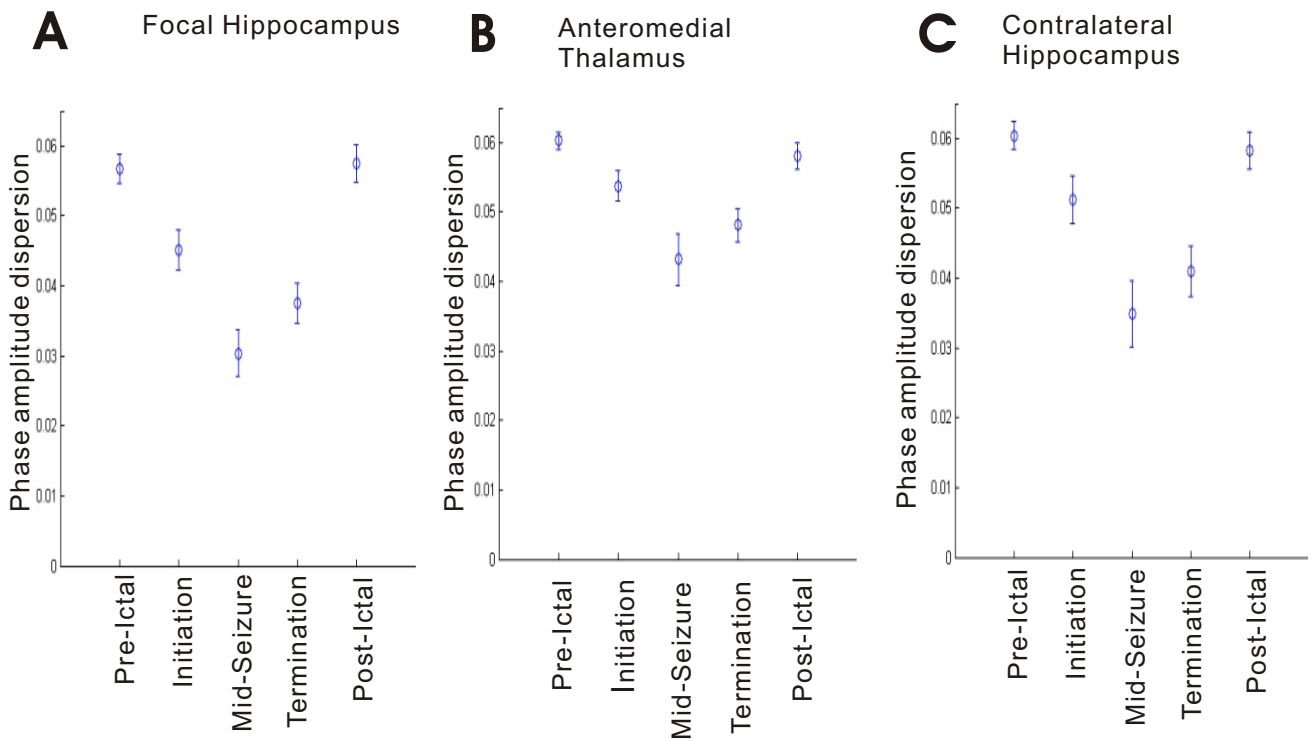


Figure 6

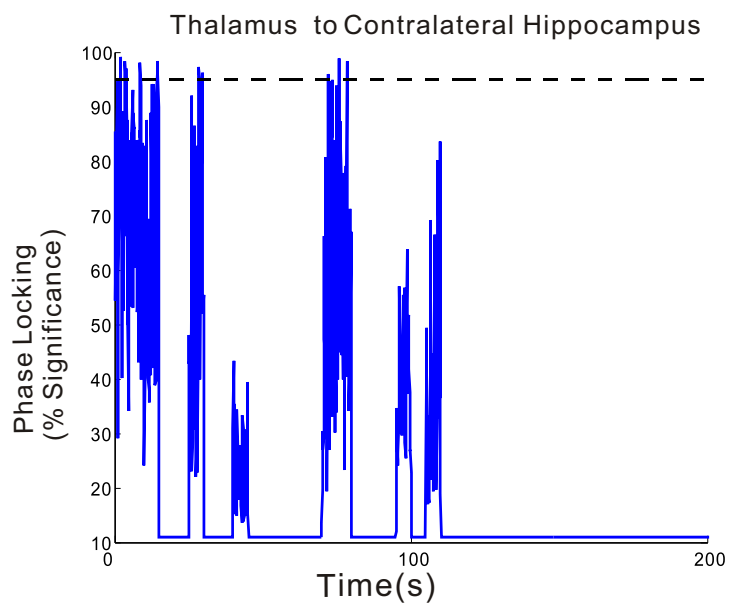
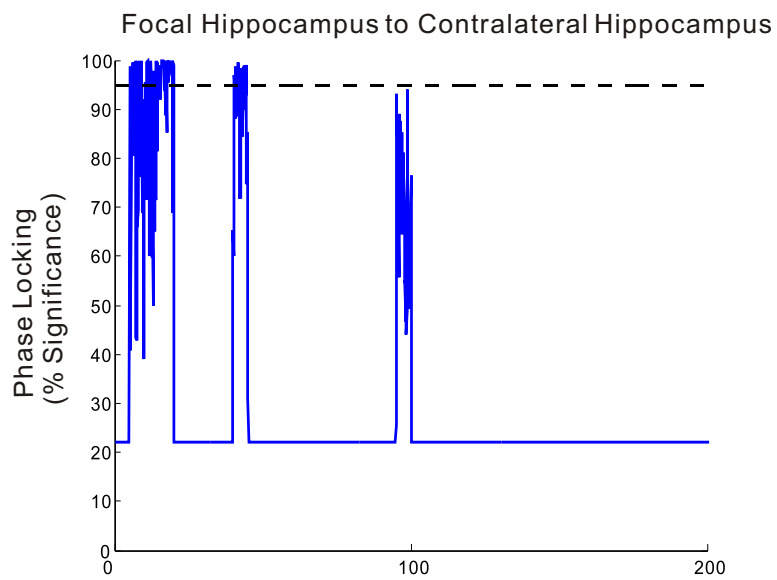
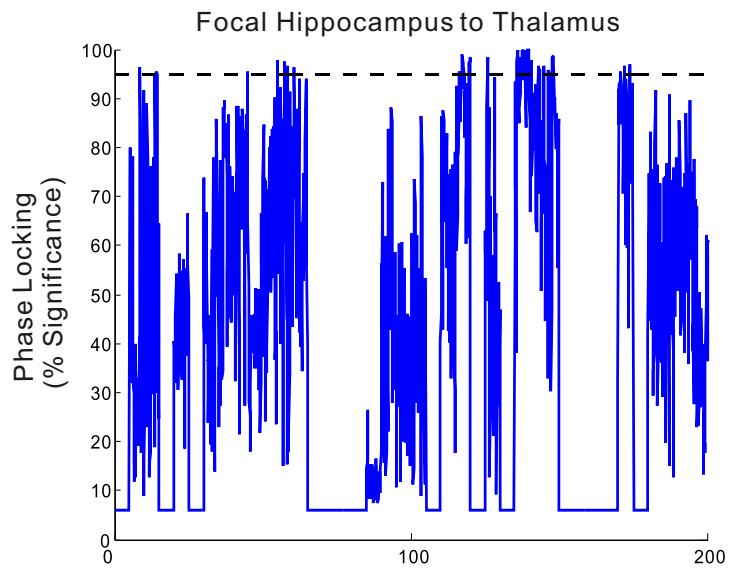
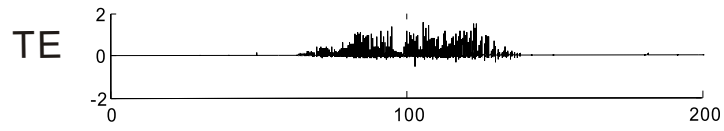


Figure 7

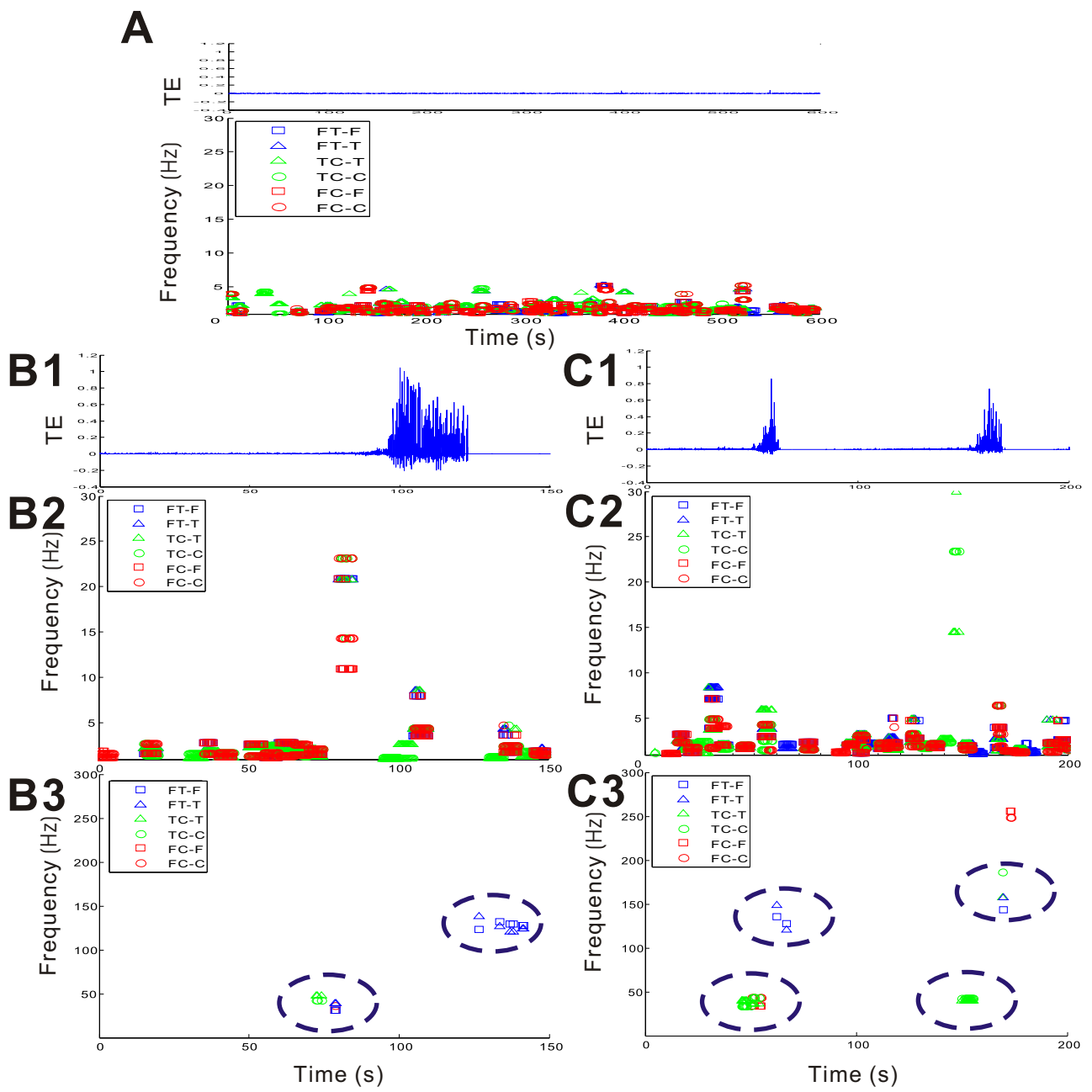
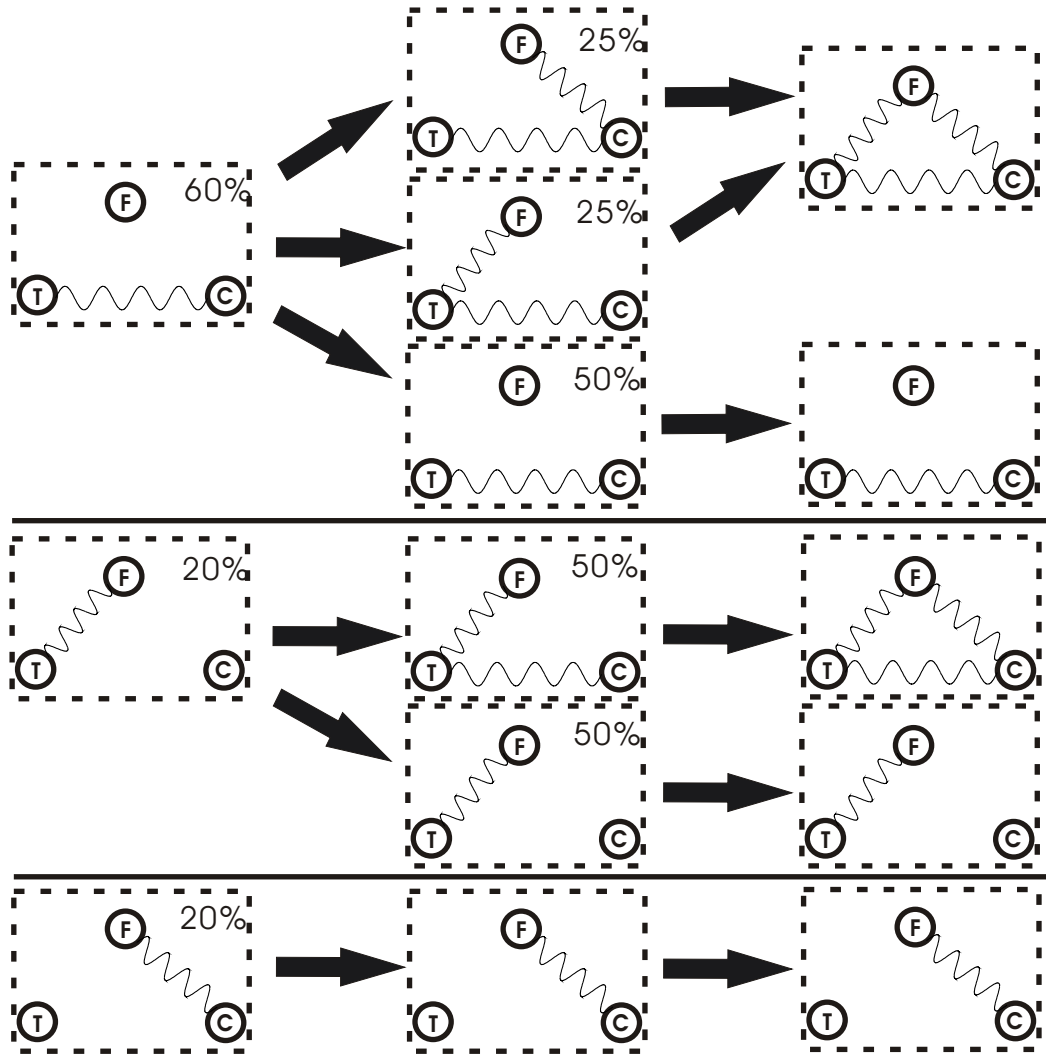


Figure 8

# A Seizure Onset



# B Seizure Termination

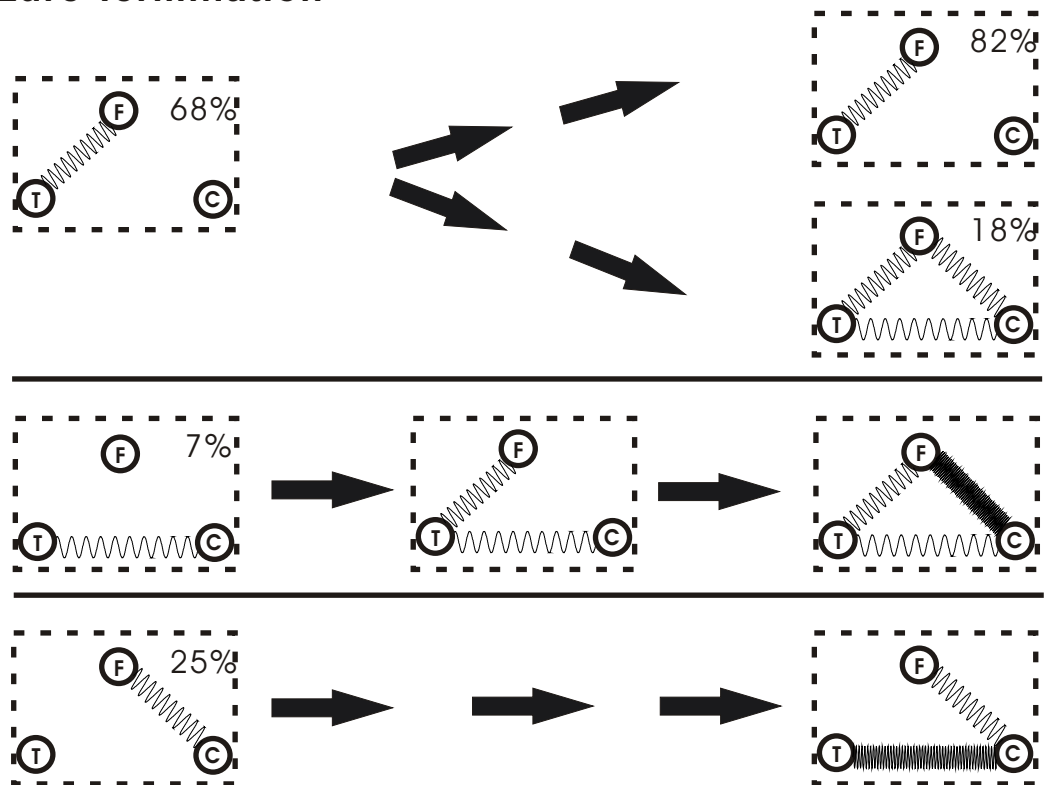


Figure 9